ENSO teleconnections in terms of non-NAO and NAO atmospheric variability

Martin P. King[1,2] · Noel Keenlyside[1,2,3,4] · Camille Li[1,2]

Abstract

The validity of the long-held understanding or assumption that El Niño-Southern Oscillation (ENSO) has a remote influence on the North Atlantic Oscillation (NAO) in the January–February–March (JFM) months has been questioned recently. We examine this claim further using atmospheric data filtered to separate the variability orthogonal and parallel to NAO. This decomposition of the atmospheric fields is based on the Principal Component/Empirical Orthogonal Function method whereby the leading mode of the sea-level pressure in the North Atlantic sector is recognised as the NAO, while the remaining variability is orthogonal (unrelated) to NAO. Composite analyses indicate that ENSO has statistically significant links with both the non-NAO and NAO variability at various atmospheric levels. Additional bootstrap tests carried out to quantify the uncertainty and statistical significance confirm these relationships. Consistent with previous studies, we find that an ENSO teleconnection in the NAO-related variability is characterised by lower-stratospheric eddy heat flux anomalies (related to the vertical propagation of planetary waves) which appear in November–December and strengthen through JFM. Under El Niño (La Niña), there is constructive (destructive) interference of anomalous eddy heat flux with the climatological pattern, enhancing (reducing) fluxes over the northern Pacific and Barents Sea areas. We further show that the teleconnection of extreme El Niño is essentially a non-NAO phenomenon. Some non-linearity of the teleconnections is suggested, with El Niño including more NAO-related variability than La Niña, but the statistical significance is degraded due to weaker signals and smaller sample sizes after the partitioning. Our findings have implications for the general understanding of the nature of ENSO teleconnections over the North Atlantic, as well as for refining methods to characterise and evaluate them in models.

1 Introduction

Understanding of El Niño-Southern Oscillation (ENSO) teleconnections in the extratropics is built on the paradigms of tropical and subtropical responses to thermal forcing in the tropical Pacific (e.g., Gill 1980; Sardeshmukh and Hoskins 1988) and the propagation of the resulting Rossby waves into the extratropics (e.g., Hoskins and Karoly 1981; Hoskins and Ambrizzi 1993; Jin and Hoskins 1995). Substantial progress in building this foundation occurred in the 1980s and 1990s (see review by Trenberth et al. 1998). Subsequent findings on the influence of the tropics on the extratropical troposphere through the stratospheric pathway contributed to new understanding of tropical-extratropical teleconnections (e.g., Bell et al. 2009; Butler et al. 2014; Cagnazzo and Manzini 2009; Garcia-Herrara et al. 2006; Garfinkel and Hartmann 2008, and the review by Domeisen et al. 2019). The stratosphere was found to play a role in the ENSO influence on North Atlantic atmospheric anomalies, through lead-lag interactions with the troposphere (same references).

Mezzina et al. (2020) questions the result from many previous studies that ENSO influences the seasonal North Atlantic Oscillation (NAO) during JFM (e.g., Bell et al. 2009; Brönnimann et al. 2007; Calvo et al. 2017; Hardiman et al. 2019; Jiménez-Esteve and Domeisen 2018; Molteni

✉ Martin P. King
martin.king@uib.no

1 Geophysical Institute, University of Bergen, Jahnebakken 5, 5007 Bergen, Norway

2 Bjerknes Centre for Climate Research, Bergen, Norway

3 Nansen Environmental and Remote Sensing Center, Bergen, Norway

4 A. M. Obukhov Institute of Atmospheric Physics, RAS, Moscow, Russia

et al. 2020; Moron and Gouirand 2003; Scaife et al. 2014; Toniazzo and Scaife 2006; Zhang et al. 2018). They examined regressions of SLP, geopotential height, zonal wind and 200 hPa-level meridional eddy heat flux (v*T*) onto indices of NAO and ENSO during JFM. Based on these, they pointed out that although the sea-level pressure (SLP) anomaly related to ENSO resembles the NAO (high spatial correlation of 0.87), there are important differences between the two phenomena at higher altitudes suggesting that the ENSO teleconnection is not connected to the NAO. In particular, the anomalies related to NAO extend further to the east over the European continent, while the ENSO teleconnection is limited to the western and central North Atlantic. However, we believe these comparisons do not detect the NAO signals effectively and there is NAO variability embedded in the ENSO teleconnections.

In this study, we examine further the result of Mezzina et al. (2020). Our main approach to the problem is to analyse separately the atmospheric variability related and unrelated to NAO. Thus, there is no ambiguity over whether a certain result involves the NAO or not. Anticipating the results, this not only clarifies our understanding of ENSO signals that are not related to NAO, it also, as we will argue, indicates that ENSO does have a role in perturbing the NAO. Analysing the ENSO-North Atlantic relationships in this way also provides insights into the distinct mechanisms and nonlinearities of the teleconnections with respect to El Niño, La Niña, and extreme El Niño events.

One mechanism of interest involves the stratospheric pathway, whose importance has been demonstrated in modelling experiments. Bell et al. (2009) found that an intermediate-complexity model simulates a clearer ENSO teleconnection to the North Atlantic if the stratospheric variability is allowed to evolve freely instead of degraded using Rayleigh drag. Other studies analysing more complex then-state-of-the-art models (e.g., Cagnazzo and Manzini 2009) also reported that 'high-top' models with better stratosphere variability produce a stronger ENSO teleconnection over high-to-mid latitudes compared to 'low-top' models. The responsible mechanism is an enhancement of the climatological lead-lag interaction between the troposphere and stratosphere. Under El Niño, vertical propagation of Rossby waves to the stratosphere and weakening of the polar vortex precede a downward signal to the troposphere that projects on the canonical negative NAO (Bell et al. 2009; Butler et al. 2014; Ineson and Scaife 2009; Jiménez-Esteve and Domeisen 2018). Generally, La Niñas are associated with the opposite effects, however some studies have reported nonlinearity in the strength of the teleconnection versus the amplitudes of the tropical Pacific SST anomaly (Iza et al. 2016).

The strongest (we use the term 'extreme', see further details in Sect. 2.3) El Niños have been found to be associated with teleconnection that does not resemble the negative NAO, but instead a southwest-to-northeast orientated Rossby wave train (Toniazzo and Scaife 2006; Scaife et al. 2017). This tropical-to-extratropical teleconnection could originate from the eastern Pacific, where SST anomaly peaks during strong El Niño, and links to the North Atlantic via the tropical Atlantic (Toniazzo and Scaife 2006; Casselman et al. 2022). By analysing tree-ring based climate reconstruction as well as data from the instrumental period, King et al. (2020) reported that the hydroclimate impacts in Europe are also different under extreme El Niños compared to regular El Niños. Given that the teleconnection to NAO is often found to be associated with the stratospheric pathway (e.g., Butler et al. 2014; Ineson and Scaife 2009; Jiménez-Esteve and Domeisen 2018), we might also speculate that the extreme El Niño teleconnection to the North Atlantic does not strongly involve the stratosphere.

Another factor in the context of nonlinearity of teleconnection is the locations of ENSO SST anomaly maxima, usually as central-Pacific (CP) versus eastern Pacific (EP) locations. Zhang et al. (2018) reported that CP ENSO teleconnection has a strong symmetry between El Niño and La Niña teleconnections, while EP La Niña teleconnection contributes to an asymmetry over the North Atlantic. They attribute this to the relatively cold climatological SST in the eastern Pacific which under EP La Niña is below the convective threshold, and only under strong enough EP El Niño that anomalous convection is triggered. A number of studies (Calvo et al. 2017; Graf and Zanchettin 2012; Ren et al. 2019) found that CP ENSO, compared to EP ENSO, has a more distinct connection to the NAO. Elucidating asymmetry between El Niño and La Nina, nonlinearities in CP and EP ENSOs, or ENSO strength are challenging using reanalysis data, even for a time period stretching back to the late nineteenth century. Therefore, studies on these questions often rely on larger model ensembles (e.g., Weinberger et al. 2019).

Section 2 of the paper describes the data, the methods for decomposing the total variability into non-NAO and NAO components, and the selections of ENSO events/years. Section 3.1 presents the main result of the paper by examining ENSO teleconnections in the non-NAO and NAO filtered data. Section 3.2 covers a few related atmospheric properties in this non-NAO/NAO perspective, while Sect. 3.3 covers aspects related to asymmetry of the teleconnections with respect to extreme El Niño, CP and EP ENSO from the perspective of non-NAO/NAO variability. Lastly, Sect. 4 summarises the results and discusses implications and unresolved issues.

2 Data and methods

2.1 Data

As in the related studies of Deser et al. (2017), King et al. (2021), and Mezzina et al. (2020), atmospheric variables such as sea-level pressure (SLP), geopotential height (Z), meridional wind (v) and air temperature (T) are taken from the NOAA-CIRES Twentieth Century Reanalysis (V2c) for the period 1851−2014 (Compo et al. 2011). Analyses on SLP and Z data are applied on 'seasonal' anomalies from the November–December (ND) or January–February–March (JFM) means. For investigating the vertical propagation of planetary waves we use the meridional eddy heat flux v*T*. The variables v and T at daily resolution are first 10-day low-pass filtered to retain the quasi-stationary variability. The deviations from zonal means for the low-pass filtered v and T are used to calculate the daily v*T*, then the ND and JFM anomalies for every year are calculated.

The sea-surface temperature (SST) data used for identifying the ENSO events are taken from HadISST1.1 (Rayner et al. 2003).

2.2 Separation of NAO and non-NAO components

We filter the total variability of the data into NAO and non-NAO components based on Principal Components (PC) of SLP in the North Atlantic sector (20°–80° N, 90° W–40° E). A two-dimensional SLP anomaly field at time t, SLP(t), can be expressed as

$$SLP(t) = \sum_{n=1}^{N} c_n(t)E_n,$$

where E_n is the nth Empirical Orthogonal Function (EOF) and $c_n(t)$ is the corresponding nth PC time series (the projection of $\boldsymbol{SLP}$ on $\boldsymbol{E_n}$ at time t). Here, $\boldsymbol{E_n}$ and $\boldsymbol{C_n}$ are computed for the ND and JFM seasons, and t in the equation above identifies a particular year. The first PC time series is regarded as the NAO index (same method as in Mezzina et al. 2020 and others) and the corresponding EOF is the well-known dipole NAO pattern (see Fig. 1d in Mezzina et al. 2020). Therefore, the portion of the SLP variability that is parallel (we also sometimes use the term 'related') to the NAO is given by:

$$SLP(t) \parallel NAO = c_1(t)E_1,$$

while the portion of SLP variability that is orthogonal to NAO (we also use the terms 'unrelated to NAO' and 'non-NAO') consists of the remaining PCs:

$$SLP(t) \perp NAO = SLP(t) - SLP(t) \parallel NAO.$$

The NAO and non-NAO separation for other fields such as the geopotential height is calculated similarly, but always using c_1 (NAO index) obtained from SLP in the North Atlantic sector so that we have just one consistent definition of the NAO. This is important as it permits interpreting the NAO or non-NAO variability across different fields, since the partitioning is always done according to the same NAO index.

With this separation, all the analyses in our study are then performed on data containing only the NAO variability or only non-NAO variability. This approach allows us to address the question of whether ENSO teleconnections are linked to the NAO in an unambiguous fashion: if no relation exists, then composites showing the ENSO teleconnection patterns made with the NAO-related data should not have any significant signal in the North Atlantic sector. Because of the linear nature of the composite analysis, the sum of the composites using the NAO and non-NAO filtered data must be equal to the composites using the original data. This has a desirable result that the contributions of the NAO and non-NAO composites to the total composites can be compared directly.

2.3 Selection of ENSO events

The central-Pacific (CP) and eastern-Pacific (EP) ENSO events are selected using the areas depicted by boxes a and b respectively (Fig. 1a, b). These areas are similar to those used by Ashok et al. (2007) to study ENSO Modoki.

CP El Niños are selected according to the following criteria:

{[SSTanom in box a] >= 0.6 K} AND

{[SSTanom in box a] > [SSTanom in box b]},

while CP La Niñas are selected according to:

{[SSTanom in box a] <= −0.6 K} AND

{[SSTanom in box a] < [SSTanom in box b]},

The SST composite for CP-El Niños minus CP-La Niñas in DJF is shown in Fig. 1a. Similarly, the EP El Niños and La Niñas are found using the following criteria, respectively:

{[SSTanom in box b] >= 0.6 K} AND

{[SSTanom in box b] > [SSTanom in box a]},

{[SSTanom in box b] <= −0.6 K} AND

{[SSTanom in box b] < [SSTanom in box a]}.

The SST composite for EP-El Niños minus EP-La Niñas in DJF is shown in Fig. 1b. An ENSO event is commonly (by e.g., NOAA, Butler et al. 2014; Weinberger et al. 2019) considered in progress, when there is a persistent SST anomaly of at least 0.5 K occurring in these regions. The threshold is set to 0.6 K here to avoid having too many events with
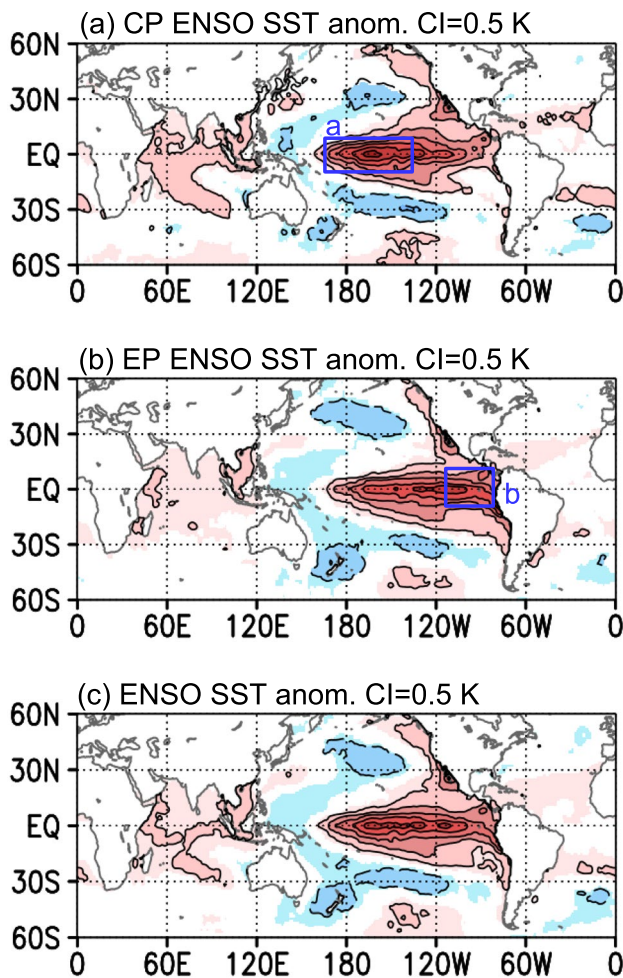
Fig. 1 SST composites for El Niño minus La Niña events in DJF. Original data: HadISST v1.1. **a** Central-Pacific ENSO, **b** eastern-Pacific ENSO, **c** both EP and CP ENSOs together. Box a covers the area 165° E–140° W, 10° S–10° N; and box b covers 110° W–80° W, 10° S–10°N. CI stands for 'contour interval'. The colour shading indicates statistical significance level at 5%, as well as with red (blue) shading for positive (negative) values

In the analyses presented in Sect. 3.1, we study the teleconnections by calculating the linear composites as atmospheric anomalies associated with El Niño minus those associated with La Niña. Our study leaves out the question of decadal-to-multidecadal modulation of teleconnection (e.g., Ivasić et al. 2021; King et al. 2018b; López-Parages and Rodríguez-Fonseca 2012; López-Parages et al. 2014) and concentrates on average composites using the entire samples. Modulations of teleconnections are generally challenging to demonstrate with high statistical confidence using sample sizes equivalent to the reanalysis period (Michel et al. 2020). The extreme El Niños have been excluded from the analyses in Sects. 3.1 and 3.2 because they are known to have a different teleconnection in the North Atlantic (King et al. 2020; Toniazzo and Scaife 2006). In Sect. 3.3 we present the effect of the extreme El Niños. We select 5 extreme events of DJF 1877/78, 1888/89, 1972/73, and 1982/83, and 1997/98 (Brönnimann et al. 2007; Toniazzo and Scaife 2006). Most of these extreme events have close to or above 2.0 K SST anomaly in the eastern Pacific (box b). Section 3.3 also presents results from investigating atmospheric anomalies associated with CP-El Niño, CP-La Niña, EP-El Niño, and EP-La Niña events separately to gauge the extent of nonlinearities in the perspective of non-NAO and NAO related variability.

3 Results

3.1 ENSO teleconnections in terms of non-NAO and NAO variability

Sections 3.1 and 3.2 present linear composites as atmospheric anomalies associated with El Niño minus those associated with La Niña. We have not found important qualitative differences between the linear atmospheric composites (El Niño minus La Niña) of CP- and EP-ENSO events, therefore these events are pooled together to increase the sample size for the composite analyses.

Composites of atmospheric fields associated with ENSO during Nov–Dec are displayed in the left columns of Figs. 2 (orthogonal to NAO) and 3 (parallel to NAO). An ENSO-related anomaly pattern that resembles the East Atlantic (EA) pattern during Nov-Dec has been reported by previous studies (Abid et al. 2021; Ayarzagüena et al. 2018; Moron and Gouirand 2003; King et al. 2018a, 2021; Molteni et al. 2020). Here, the analysis indicates that this ENSO teleconnection to the EA-like pattern is from the portion of the variability that is orthogonal to the NAO (top row in Fig. 2). Additionally, analysis of the variability parallel to NAO finds that El Niño (La Niña) is connected to the positive (negative) phase of the NAO (top row in Fig. 3) during Nov–Dec (see also Molteni et al. 2020).

weak teleconnections, while at the same time not reducing the number of events (sample size) adversely (King et al. 2021). The resulting uncertainty in the teleconnection from this choice is quantified using bootstrap tests in Sect. 3.1.

The corresponding SST composite for these two types (i.e., CP and EP) of ENSO anomalies grouped together (resulting in 23 El Niño and 33 La Niña events in DJF, see supplementary Table 1) has a pattern that resembles the canonical ENSO SST anomaly obtained using the Niño3.4 index (Fig. 1c). Following the same approach in Deser et al. (2017) and King et al. (2021), ENSO events for DJF (OND) are used for selecting lagged JFM (ND) atmospheric fields. The various types of ENSO events for DJF and OND identified are listed in supplementary Table 1.

Fig. 2 Atmospheric fields composites for El Niño minus La Niña events (EP- and CP-ENSO are pooled together, extreme El Ninos are excluded). The variability orthogonal to NAO is analysed here. Blue (red) contour lines indicate negative (positive) anomalies. The grey shading indicates statistical significance level at 5%. Original data: NOAA-CIRES Twentieth Century Reanalysis (V2c)
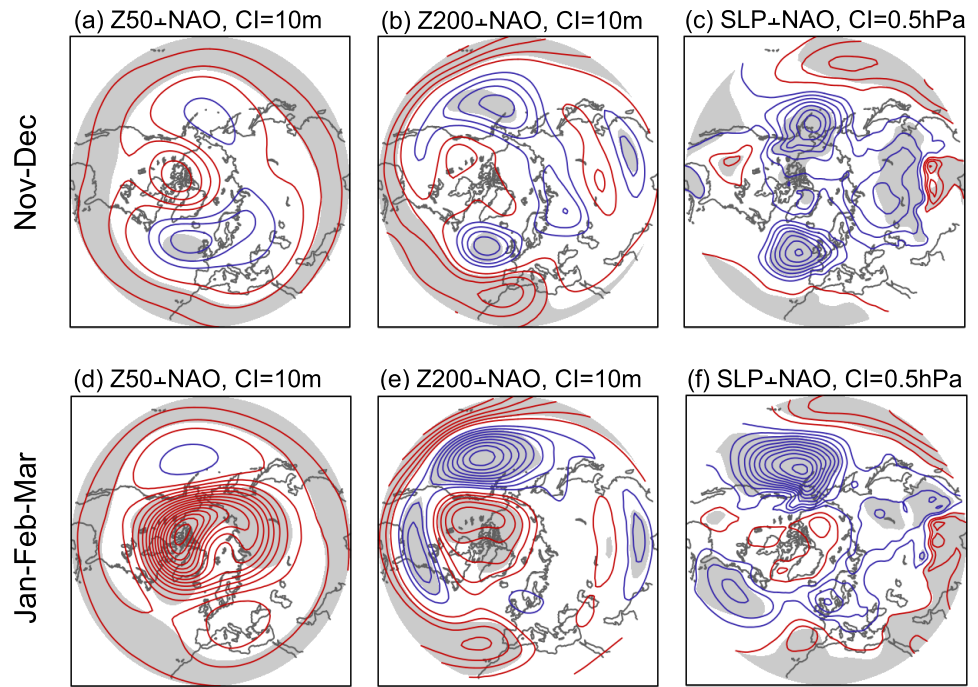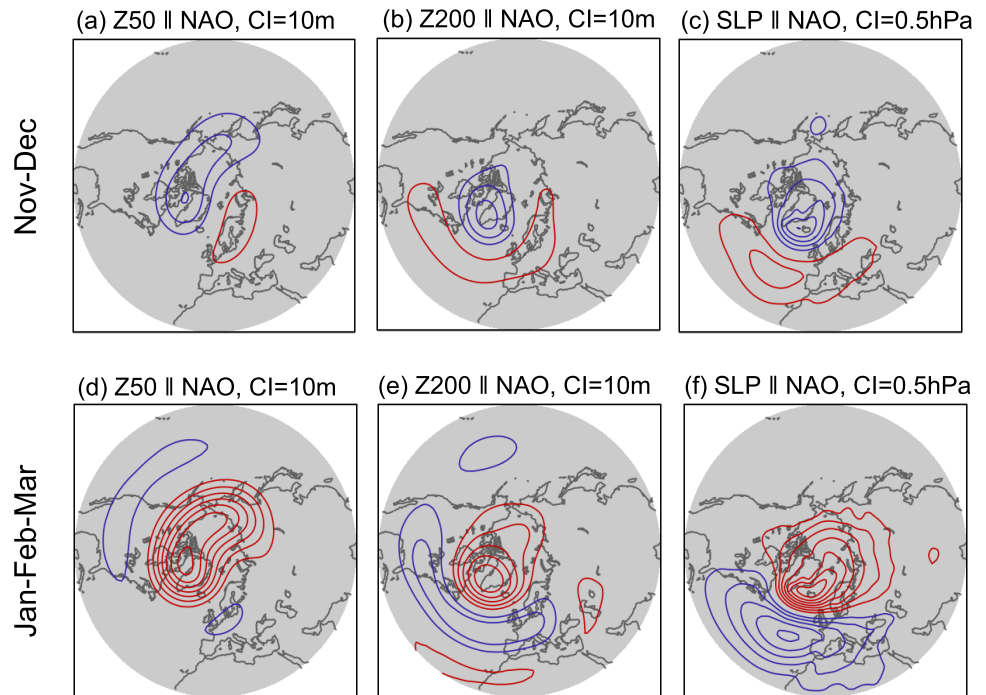

(a) Z50⊥NAO, CI=10m   (b) Z200⊥NAO, CI=10m   (c) SLP⊥NAO, CI=0.5hPa

Nov-Dec

(d) Z50⊥NAO, CI=10m   (e) Z200⊥NAO, CI=10m   (f) SLP⊥NAO, CI=0.5hPa

Jan-Feb-Mar

Fig. 3 Atmospheric fields composites for El Niño minus La Niña events (EP- and CP-ENSO are pooled together, extreme El Niños are excluded). The variability parallel to NAO is analysed here. Blue (red) contour lines indicate negative (positive) anomalies. The grey shading indicates statistical significance level at 5%. Original data: NOAA-CIRES Twentieth Century Reanalysis (V2c)

(a) Z50 ∥ NAO, CI=10m   (b) Z200 ∥ NAO, CI=10m   (c) SLP ∥ NAO, CI=0.5hPa

Nov-Dec

(d) Z50 ∥ NAO, CI=10m   (e) Z200 ∥ NAO, CI=10m   (f) SLP ∥ NAO, CI=0.5hPa

Jan-Feb-Mar

Results addressing the main focus of this study are shown in the bottom rows in Figs. 2 and 3. Composites of the non-NAO variability in JFM associated with ENSO (Fig. 2e, f) show the well-known arching wavetrain from the North Pacific (e.g., Ayarzagüena et al. 2018; Butler et al. 2014; Trenberth et al. 1998 and references therein), with the prominent feature being a weakening of the Aleutian Low. Composites of the NAO-related variability (Fig. 3e, f) are also consistent with the conventional thinking of a negative (positive) NAO being associated with El Niño (La Niña). The amplitudes of the SLP linear composites shown in Fig. 2f, 3f indicate that the average El Niño and La Niña teleconnection over the North Atlantic and Europe is at 20–30% of one standard deviation of the SLP anomalies

in the region (figure not shown). Thus, while the non-NAO variability dominates over the North Pacific, both non-NAO and NAO variability are important for the ENSO teleconnection over the North Atlantic. Note that by definition, the sum of the non-NAO and NAO composites must be equal to the composite from the original data (where non-NAO vs NAO filtering is not applied), and Fig. 10 confirms this relationship (as well as verifying that our calculations have been done correctly). To illustrate our reasoning further, Fig. 10 also indicates that although the upper tropospheric composite using the original (Fig. 10d) data is hemispherically very similar to that using the data filtered to retain variability orthogonal to NAO (Fig. 10a), there is in fact an NAO-related pattern embedded (Fig. 10c and d are identical), which might not be recognised readily if only the original data are examined. The inclusion of extreme El Niño events in the composites would strengthen the non-NAO pattern and thus weaken the contribution of the NAO signal to the overall teleconnection (we explore this further in Sect. 3.3), but not so much that the NAO should be disregarded (not shown). Thus, our analysis shows statistically significant ENSO teleconnections related to NAO throughout the depth of the troposphere (Fig. 3e, f).

Since the data used in the analysis for Fig. 3 contains only the NAO variability, a reasonable criticism is that any selection of anomalies to calculate the composites must only result in either positive *or* negative NAO, regardless of whether there is any statistical significance. Therefore, in addition to the Student's *t* test already shown in Fig. 3e, f we have performed two bootstrapping tests to evaluate the robustness of the signs and amplitudes. The first test is similar to the one used in Deser et al. (2017) and King et al. (2021). To obtain a bootstrap NAO index related to ENSO, the El Niño and La Niña years are, respectively, randomly sampled with replacement; and the difference (El Niño minus La Niña) in the mean standardised PC 1 (NAO index) values is then calculated. This step is repeated 20,000 times to create a range of bootstrap values. The resulting 2.5th-to-97.5th percentile confidence interval (which quantifies the uncertainty in sampling) contains only negative values of NAO index (Fig. 4a). Panels c, d show the corresponding SLP anomalies for these percentiles, indicating spatially the negative NAO at these limits. The result of the test confirms the statistical significance shown in Fig. 3f and the notion of ENSO's relationship with the sign of NAO that is consistent with conventional understanding. Molteni et al. (2020) also bootstrapped the CERA-20C reanalysis and found that the ENSO-related NAO index defined based on 500 hPa geopotential height spans negative values during the January–February months, thus providing additional support.

The second test implements a bootstrap test in which all the available JFM seasons in the period 1870 to 2014 are used for calculating 23 randomly drawn seasons minus 33 randomly drawn seasons. The null hypothesis is that the selected El Niño and La Niña events are random samples as far as the hypothesised teleconnection to NAO is concerned, and therefore the calculated teleconnection has no statistical significance. A smaller bootstrap sample size (2000) is produced here because sampling of spatial data is more computationally intensive compared to sampling of indices above. The grey shading in the left (right) column Fig. 11 indicates grid-points where the observed composites (as shown in Fig. 3e, f) are less (greater) than the 5th (95th) percentile grid-point values of the bootstrap composites. Together these also mean there are less than 5% of the random samples have negative (positive) anomalies as low (high) as the southern (northern) centre of action in the observed composites. In other words, the null hypothesis can be rejected and the hypothesis that the El Niño minus La Niña teleconnection is associated with negative NAO as shown in Fig. 3 is preferred at a 95% confidence level.
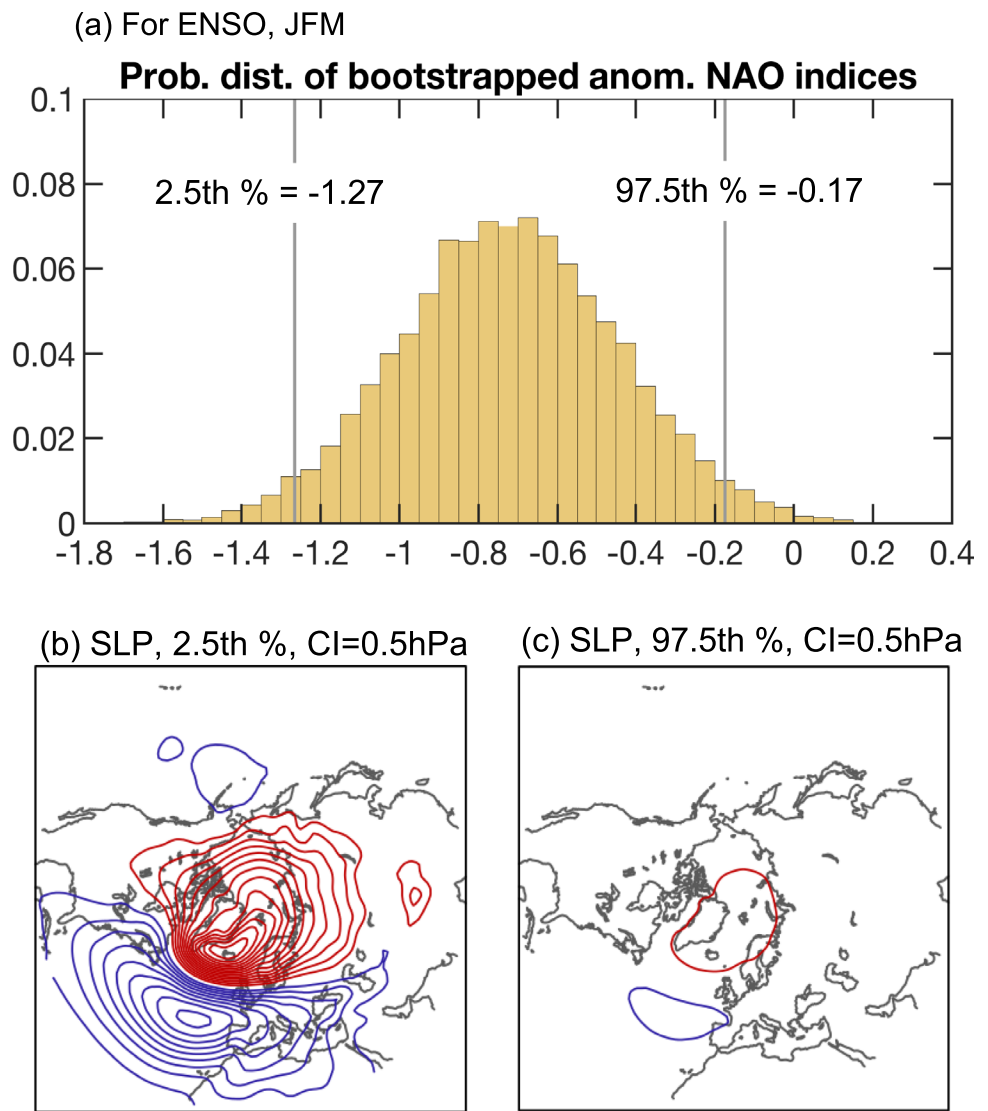
Finally, we note that the anomalies shown in Fig. 3 are a spatial representation of the relationship between ENSO and the NAO index (PC 1) because all the points in space co-vary mutually and perfectly with the NAO index (correlation coefficient = 1.0). There is effectively only one degree of freedom in space for the NAO-related data. If there is a statistical significance in the relationship between ENSO and the NAO index, then there is statistical significance for all grid points (local significance); and as we shall see later if there is no statistical significance, it is also absent in all grid points. In this case, a global (i.e., field) statistical significance test is equivalent to the local test, and the two have the same *p* values (< 0.05). Attaining the field significance here would not add further statistical confidence than the local test already provides. It is not trivial to avoid this issue in investigating ENSO's link to NAO explicitly, as this investigation relies on a definition of NAO that is essentially based on a time series and statistical detection of a signal in this 'noisy' time series. However, the three statistical tests (Student's t and two bootstrap tests) carried out above help to improve confidence in the identified ENSO-NAO relationship.

3.2 Related atmospheric properties

In this section, we describe other preceding and contemporaneous atmospheric properties associated with ENSO teleconnection in terms of the variability orthogonal and parallel to NAO in JFM.

To examine the composite patterns that precede JFM teleconnection, we show in top and bottom rows in Fig. 5 the ENSO composites for Nov–Dec anomalies which are unrelated and related, respectively, to NAO in JFM. These composite patterns in Fig. 5 lead the ones in JFM (bottom rows of Figs. 2, 3 respectively) by approximately two

Fig. 4 **a** Probability histogram of 20,000 bootstrapped anomalous NAO (PC 1) indices associated with ENSO (El Niño minus La Niña) for JFM. Each anomalous NAO index is the mean PC 1 value from bootstrapping 23 El Niños minus the mean PC 1 value from bootstrapping 33 La Niñas, this is repeated 20,000 times. The grey vertical lines and labels indicate the 2.5th and 97.5th percentiles. The pattern in Fig. 3i corresponds to anomalous NAO index of about −0.7. **b** The SLP composite corresponding to 2.5th percentile of the bootstrapped NAO indices. **c** Same as (**b**) except for the 97.5th percentile. The data parallel to NAO is shown here. Blue (red) contour lines indicate negative (positive) anomalies. Original data: NOAA-CIRES Twentieth Century Reanalysis (V2c)

(a) For ENSO, JFM

Prob. dist. of bootstrapped anom. NAO indices

2.5th % = -1.27   97.5th % = -0.17

(b) SLP, 2.5th %, CI=0.5hPa

(c) SLP, 97.5th %, CI=0.5hPa

months, if the centres of the periods are considered as reference points. The two-month-lead patterns (bottom row of Fig. 5) are fundamentally different from the zero-lag patterns (bottom row of Fig. 3), suggesting that they could be an ENSO-related precursor to the NAO in JFM. In particular, Fig. 5e, f resembles the Scandinavian or Urals blocking pattern (Barnston and Livezey 1987; Bueh and Nakamura 2007), which has been reported by previous studies to lead the NAO or Arctic Oscillation (Kuroda and Kodera 1999; Takaya and Nakamura 2008). Studies of other teleconnection drivers on NAO such as Arctic sea ice, Eurasian snow cover, and North Atlantic SST (e.g.,García-Serrano et al. 2015; Gastineau et al. 2017; Siew et al. 2020) find similar precursory circulation anomalies.

Conversely, in the case of variability orthogonal to NAO, the zero-lag (top row in Fig. 2) and 2-month-lead (top row in Fig. 5) composites in Nov–Dec have qualitatively similar patterns, both resembling the East Atlantic pattern over

the North Atlantic. Therefore, we are not able to speculate if these preceding (at 2-month-lead) atmospheric patterns have any dynamical link to the teleconnection in JFM or we are just detecting the same ENSO signals as the zero-lag composites. There is also no statistically significant signal in the stratosphere (Figs. 2a, 5a), which is normally believed to provide a dynamical pathway for a lagged correlation in JFM over the North Atlantic and projects on NAO variability. These factors together with a relative lack of prior understanding in the lead-lag mechanism for the non-NAO variability hinders our ability to infer a dynamical link in this case.

In order to gain some information about the link between the troposphere and stratosphere, Fig. 6 presents similar composite analyses for the meridional eddy heat flux (v^*T^*) in the lower stratosphere (100 hPa) leading (left column) and contemporaneous with (right column) the JFM variability. The variable v^*T^* is related to the

Fig. 5 Atmospheric fields composites for El Niño minus La Niña events (EP- and CP-ENSO are pooled together, extreme El Ninos are excluded). The top (bottom) row is for ND fields with variability orthogonal (parallel) to NAO in JFM. Blue (red) contour lines indicate negative (positive) anomalies. The grey shading indicates statistical significance level at 5%. Original data: NOAA-CIRES Twentieth Century Reanalysis (V2c)
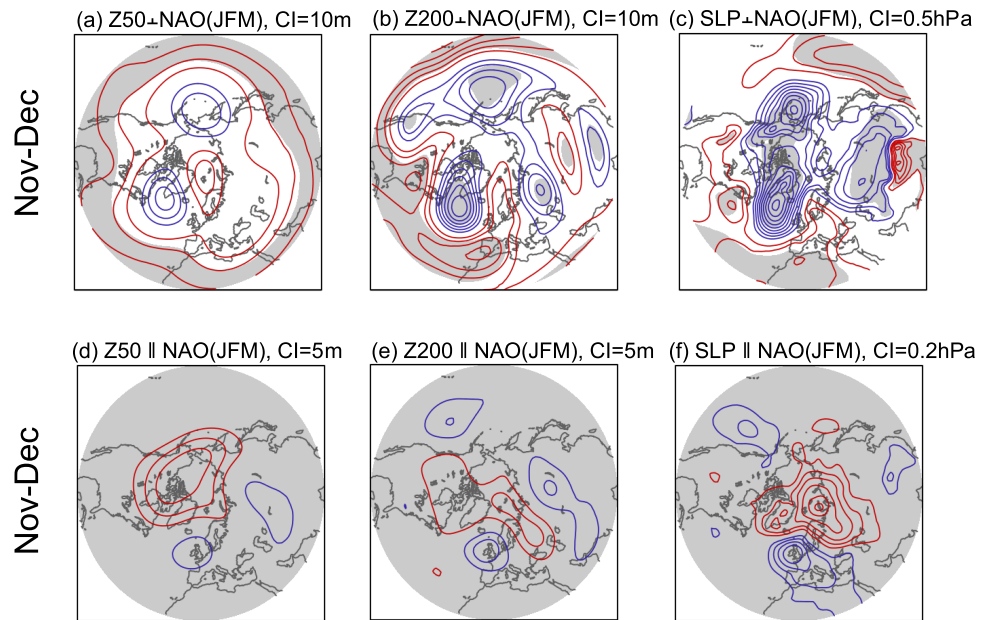
(a) Z50⊥NAO(JFM), CI=10m (b) Z200⊥NAO(JFM), CI=10m (c) SLP⊥NAO(JFM), CI=0.5hPa

Nov-Dec

(d) Z50 ∥ NAO(JFM), CI=5m (e) Z200 ∥ NAO(JFM), CI=5m (f) SLP ∥ NAO(JFM), CI=0.2hPa

Nov-Dec

Fig. 6 Shading shows composites of (top) non-NAO and (bottom) NAO related $v*T*$ at the 100 hPa level for El Niño minus La Niña events. EP- and CP-ENSO are pooled together, extreme El Niños are excluded. The left panels are ND fields with variability **a** orthogonal and **c** parallel to NAO in JFM (i.e. leading in time), while panels **b**, **d** are JFM atmospheric fields orthogonal and parallel respectively to the contemporaneous NAO. Dark contours are $v*T*$ climatologies for the respective months (Cont. Int. = 10 km/s). The curve in the side inset shows the zonal-mean values of the $v*T*$ composites along 40°–90° N, and the number atop is the mean value for this curve. Original data: NOAA-CIRES Twentieth Century Reanalysis (V2c)

Nov-Dec

Jan-Feb-Mar

(a) v*T*⊥NAO(JFM)

0.049

(b) v*T*⊥NAO

1.67

(c) v*T*∥ NAO(JFM)

0.33

(d) v*T* ∥ NAO

0.63
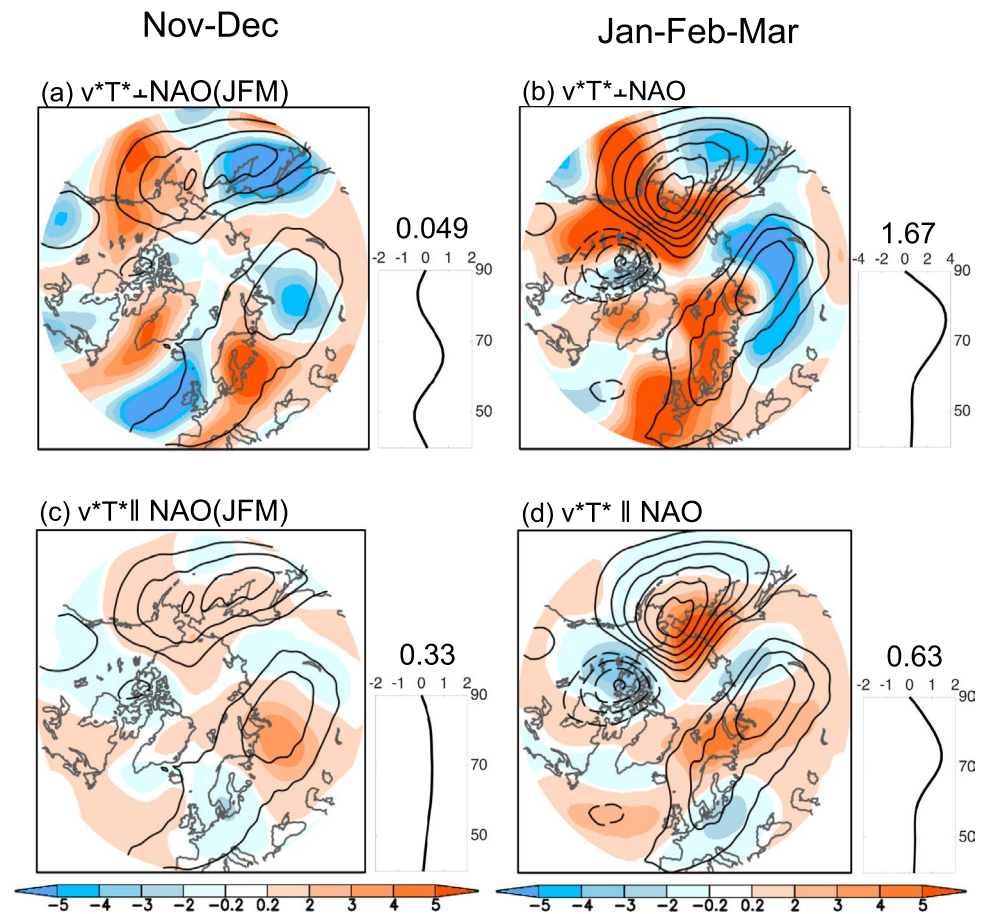
vertical propagation of planetary waves (in the framework of the zonal-mean Eliassen-Palm flux): In the zonal mean framework, an upward (downward) EP flux anomaly is usually accompanied by convergence (divergence) of the eddy fluxes in the stratosphere and therefore deceleration (acceleration) of the stratospheric polar vortex. Leading

anomalous v*T* in Nov–Dec (left column) is qualitatively similar in space to the contemporaneous anomalies in JFM (right column), but much weaker. For the non-NAO-related ENSO teleconnection, the net zonal-mean v*T* in late autumn is comparatively close to zero (side inset in Fig. 6a), which is consistent with the lack of statistically significant anomaly in the stratospheric circulation anomaly (Fig. 5a). The v*T* for non-NAO-related teleconnection only becomes stronger in the contemporaneous composite shown in Fig. 6b. In contrast, the preceding zonal mean v*T* for NAO-related ENSO teleconnection is already weakly positive in the zonal-mean (inset in Fig. 6c) and becomes stronger in the contemporaneous composite (Fig. 6d). As for the previous two paragraphs, we interpret this result as a stronger lead-lag relationship between troposphere and stratosphere exists for the NAO-related variability, but not the non-NAO variability.

We find that the contemporaneous (i.e., zero lag) anomalous v*T* has strong zonal-mean positive values (in the same sense as El Niño) for both the non-NAO and NAO variability (see side insets in the right column of Fig. 6). This is consistent with Figs. 2d, 3d, where strong anomalous positive geopotential heights in the polar stratosphere are observed. The analysis on non-NAO and NAO-related v*T* broadly agrees with previous studies which have reported enhanced (weakened) upward wave propagation over the North Pacific under El Niño (La Niña) conditions (Ineson and Scaife 2009; Jiménez-Esteve and Domeisen 2018; Manzini et al. 2006; Taguchi and Hartmann 2006). However, some further qualitative spatial details emerge here. For example, the NAO-related variability is mostly in phase with, and enhances, the climatological v*T* pattern (Fig. 6d); and in addition to the Nort Pacific, the positive v*T* over the Barents Sea and northwestern Russia also contributes to the positive zonal mean v*T* (see also Garfinkel et al. 2010; Kuroda and Kodera 1999; Peings 2019; Takaya and Nakamura 2008; White et al. 2019). The non-NAO variability (Fig. 6b) is different from this, with both anomalous positive and negative v*T* (shading) sitting across the positive climatological v*T* regions (solid contours) over the North Pacific and Eurasia. In both cases the positive v*T* anomalies are stronger than the negative anomalies, contributing to positive net zonal mean values (insets in Fig. 6b, d). We interpret the result of Fig. 6b as indicating the JFM tropospheric eddies for the non-NAO case are able to generate the anomalous upward propagating waves in the zonal mean, resulting in a strongly positive anomalous Z50 at zero-lag (see Fig. 2d). For the NAO case, the zero-lag anomalous Z50 is also positive, but is weaker (Fig. 3d), which is consistent with the weaker zonal-mean v*T* shown in Fig. 6d. Taken together, results in this section support the idea of a stratospheric pathway in the NAO-related response to ENSO, where the link with

the troposphere is already developing in Nov–Dec (Fig. 6c and bottom row in Fig. 5).
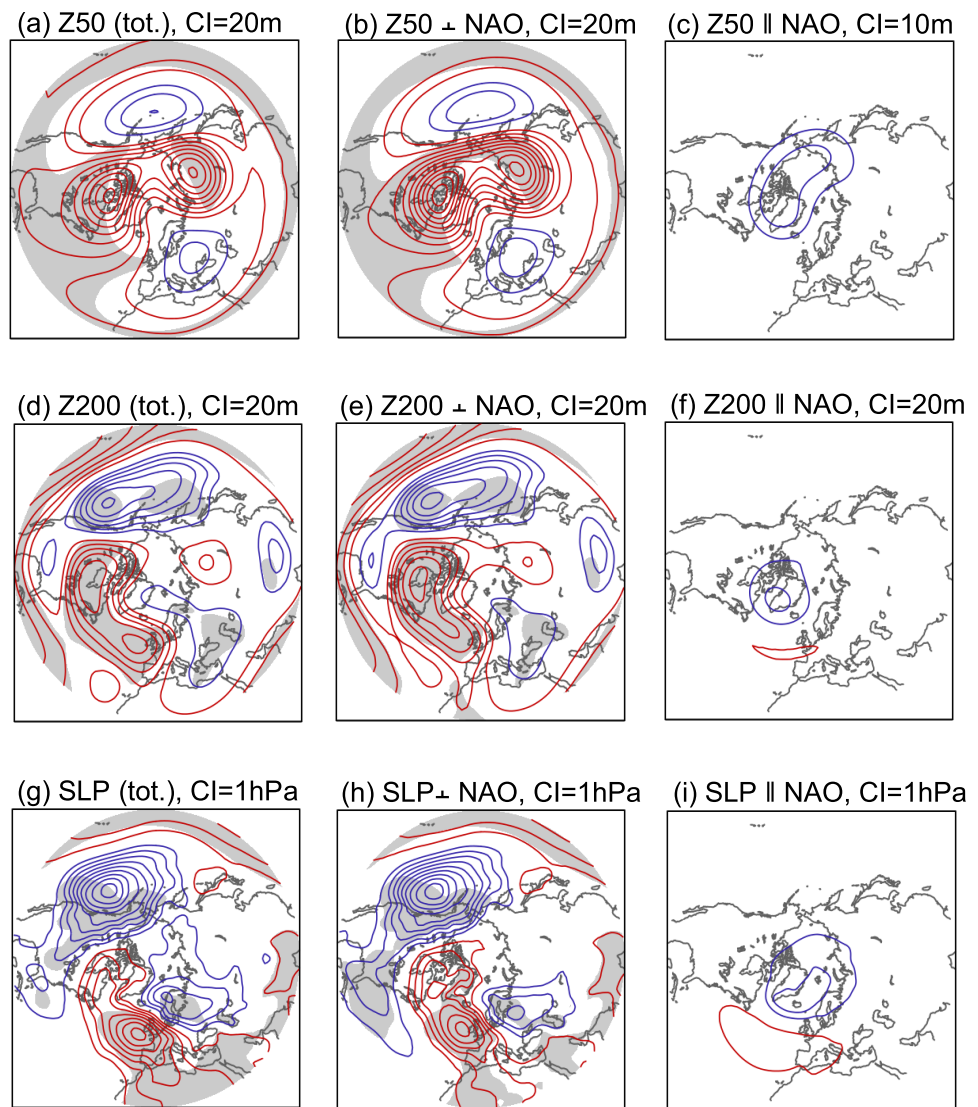
3.3 Extreme El Niños, central-pacific, and eastern-pacific ENSO teleconnections

Studies which analyse DJF or DJFM means may detect nonlinearity in teleconnections because of the existence of varying teleconnections within these months (Figs. 2, 3, also Moron and Gouirand 2003; King et al. 2018a, 2021). In this section, we briefly revisit two other factors that contribute to nonlinearities—extreme El Niños, and central tropical Pacific (CP) or eastern tropical Pacific (EP) SST anomalies—using the approach of formal separation into non-NAO and NAO components, as above. Note that all the separations (into non-NAO/NAO, El Niño/La Niña, and CP/EP ENSO) split the teleconnection signals and/or reduce the sample sizes, both of which affect the statistical significance. Therefore an important (and general) caveat here is that the lack of statistical significance may not indicate the absence of nonlinearity, only that it cannot be detected in the reanalysis data (King et al. 2021). The nonlinearity itself is a lower-order effect (a difference in the teleconnection anomalies). For these reasons, many studies on this topic rely on large ensembles of model simulations, and comment on the challenge of detecting significant nonlinearity even in these datasets (e.g., Weinberger et al. 2019). Some of the following results are not immune from this problem.

Teleconnection in the North Atlantic during JFM for the most extreme El Niño events has been found to be different from the negative NAO associated with typical El Niños (Toniazzo and Scaife 2006). For the extreme El Niños in Jan-Feb of 1983 and 2016, a seasonal forecast model (UK Met Office GloSea5) was able to simulate the anomalous SLP pattern that is similar to observations(Scaife et al. 2017). In our study, other than separation of extreme El Niños from typically strong El Niños, we do not further investigate the amplitudes of the teleconnection versus El Niño SST anomaly strengths which could be anyway challenging to establish using reanalysis data due to the limitation in sample size (but see model study of Jiménez-Esteve and Domeisen 2020).

The analysis in Fig. 7 indicates that the extreme El Niño teleconnection is completely unrelated to the NAO, unlike the regular El Niño teleconnection, which includes both non-NAO and NAO-related signals. In the left column are the composites using the original (unfiltered to non-NAO vs. NAO variability) data, and the middle and right columns are, respectively, the composites from the non-NAO and NAO variability. The extreme El Niño teleconnection obtained here (left column) agrees with Toniazzo and Scaife (2006). By definitions of our methods, the sum of the middle and

Fig. 7 Atmospheric field composites in JFM for extreme El Niño events (1878, 1889, 1973, 1983, 1998). Composites are calculated using Left: the original unfiltered data, middle: data containing variability orthogonal to NAO, right: data containing variability parallel to NAO. Blue (red) contour lines indicate negative (positive) anomalies. The grey shading indicates statistical significance level at 5%. Original data: NOAA-CIRES Twentieth Century Reanalysis (V2c)

(a) Z50 (tot.), CI=20m   (b) Z50 ⊥ NAO, CI=20m   (c) Z50 ‖ NAO, CI=10m

(d) Z200 (tot.), CI=20m   (e) Z200 ⊥ NAO, CI=20m   (f) Z200 ‖ NAO, CI=20m

(g) SLP (tot.), CI=1hPa   (h) SLP⊥ NAO, CI=1hPa   (i) SLP ‖ NAO, CI=1hPa

right panels in each row must be equal to the left panel. So Fig. 7 confirms that the non-NAO variability (middle column) dominates the total composites, while NAO-related signals (right column) are very weak and not statistically significant.

The composites for Nov–Dec fields under the same extreme El Niño events (Fig. 12, about 2 months lagged composites) also show the dominance of the preceding non-NAO variability. Interestingly, there are similarities between the teleconnection anomalies for the extreme El Niño (Fig. 7, left column) and the non-NAO-related teleconnections shown in Fig. 2 and top row of Fig. 5 for typical (i.e., 'non-extreme') El Niños, suggesting that the anomalies observed under extreme El Niños could be still active under typical El Niños. The two differences are that, under typical El Niños, the variability orthogonal to NAO is weaker than that under extreme El Niños (note that in Figs. 7, 12 the contour intervals used are twice those in Fig. 2), and

the NAO-related variability is also active. Why in the first place extreme El Niños amplify the non-NAO and have no influence on the NAO variability of the teleconnection is an interesting question for further research. Toniazzo and Scaife (2006) suggests that forcing from the tropical Atlantic that covaries with El Niño plays a role in this. We also note that there is a stronger and statistically significant anomaly in the stratosphere over far-eastern Russia during Nov–Dec under extreme El Niños (Fig. 12b), but this feature is absent or weak under typical El Niños (Fig. 5a). Hardiman et al. (2019) report that the tropospheric pathway of ENSO teleconnection (based on Rossby wave sources over the Caribbean and tropical Atlantic) is linear with the ENSO index, thus intensifying the non-NAO teleconnection for an extreme ENSO event.

For completeness, Fig. 13 documents the v^*T^* at 100 hPa level related to extreme El Niños in JFM, corresponding

to Fig. 6 for the 'non-extreme' ENSO events. One notable point here is that the contemporaneous v*T* for non-NAO

El Nino   La Nina

(a) Z200⊥NAO, CI=10m   (b) Z200⊥NAO, CI=10m

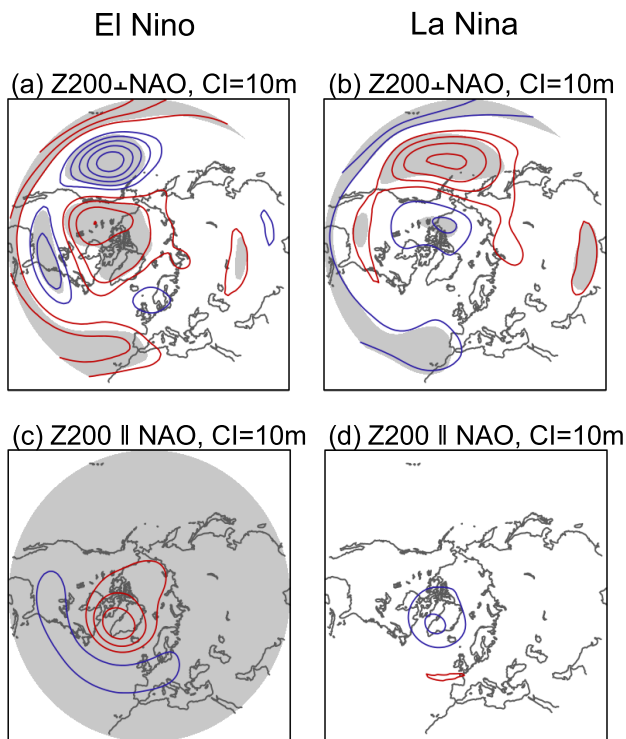(c) Z200 ‖ NAO, CI=10m   (d) Z200 ‖ NAO, CI=10m

Fig. 8 Z200 composites under El Niño (left) and La Niña (right) in JFM. EP and CP events are considered together, extreme El Niños are excluded. Top: variability orthogonal to NAO, bottom: variability parallel to NAO. Blue (red) contour lines indicate negative (positive) anomalies. The grey shading indicates statistical significance level at 5%. Original data: NOAA-CIRES Twentieth Century Reanalysis (V2c)

variability (Fig. 13b) has very large values, which is also consistent with the strong Z50 anomaly seen in Fig. 7b, while the composite related to NAO is very weak comparatively (Fig. 13d), with no statistically significant signal in the stratosphere (Fig. 7c). The preceding v*T* in Nov–Dec (Fig. 13a, c) is also weak, again consistent with weak or no signals in the preceding Z50 (Fig. 12b, c) for the NAO-related variability.

Nonlinearity or asymmetry is an important topic in ENSO teleconnections research. In this final part, we briefly examine the teleconnections due to El Niño and La Niña separately, including their CP and EP counterparts, from the non-NAO and NAO perspective. Although there are localised differences in the anomalies, considering only the overall signs and patterns in the whole hemisphere (or the North Pacific or Atlantic sectors separately) indicates no noteworthy asymmetry between El Niño and La Niña's teleconnections (Fig. 8) (see also e.g. Bayr et al. 2019; Deser et al. 2017; Hardiman et al. 2019; King et al. 2021; Toniazzo and Scaife 2006). The non-NAO signal for La Niña (Fig. 8b) is slightly weaker than for El Niño (Fig. 8a). The NAO-related ENSO signal in the upper troposphere (Fig. 3e) turns out to come primarily from El Niño (Fig. 8c), with the La Niña signal being much weaker, and in fact not statistically significant on its own (Fig. 8d). Iza et al. (2016) found that stronger La Niña SST anomalies are required compared to El Niño to obtain North Atlantic teleconnection of equivalent magnitude, indicating nonlinearity between amplitudes of teleconnection anomaly over the North Atlantic and ENSO strengths (see also Jiménez-Esteve and Domeisen 2020).

In terms of CP and EP event, Fig. 9 indicates no major asymmetry of note, considering the signs and patterns broadly over the whole hemisphere and only the statistically
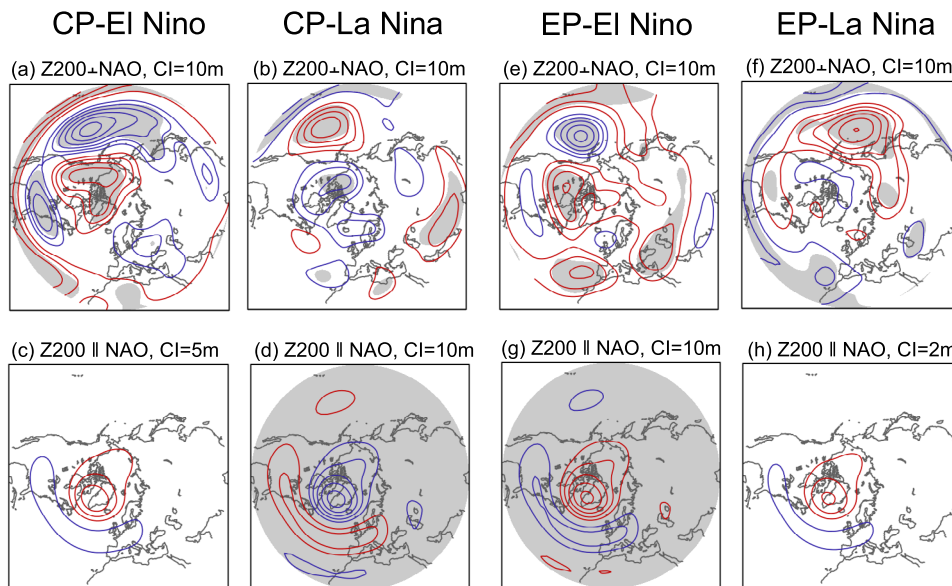
Fig. 9 Z200 composites under CP-El Niño (1st col), CP-La Niña (2nd col), EP-El Niño (3rd col), and EP-La Niña (4th col) in JFM, extreme El Niños are excluded. Top: variability orthogonal to NAO, bottom: variability parallel to NAO. Blue (red) contour lines indicate negative (positive) anomalies. The grey shading indicates statistical significance level at 5%. Original data: NOAA-CIRES Twentieth Century Reanalysis (V2c)

CP-El Nino   CP-La Nina   EP-El Nino   EP-La Nina

(a) Z200⊥NAO, CI=10m   (b) Z200⊥NAO, CI=10m   (e) Z200⊥NAO, CI=10m   (f) Z200⊥NAO, CI=10m

(c) Z200 ‖ NAO, CI=5m   (d) Z200 ‖ NAO, CI=10m   (g) Z200 ‖ NAO, CI=10m   (h) Z200 ‖ NAO, CI=2m

significant signals. A number of previous studies (e.g., Feng et al. 2017; Zhang et al. 2018) reported nonlinearity in the North Atlantic-European sector due to EP-La Niña. Our analysis here reveals that this nonlinearity originates from the NAO component (Fig. 9h), where EP-La Niña teleconnection has opposite signs to CP-La Niña, and also to what is expected under La Niña in general. However, an important caveat is that the anomaly in Fig. 9h is not statistically significant by itself, although it does contribute to the apparent nonlinearity in some analyses. Regionally, for the signals orthogonal to the NAO, EP events have teleconnections that extend into the midlatitude Atlantic and reach the Iberian peninsula (Fig. 9e, f), while this is not the case for the CP events (Fig. 9a, b).

By definition of the EOF method, the NAO and non-NAO components are not temporally correlated when considering the entire analysis period. One could ask if this is still true within a selected subset of the data, where the defined NAO and non-NAO variability could be correlated, whether by chance or due to other influences. However, we find no such correlation between the non-NAO and NAO variability for the North Atlantic sector across our selected ENSO events (not shown). In other words, the non-NAO and NAO anomalies still do not occur together on average during the ENSO years. This leads to an important question on which factors determine whether the non-NAO or NAO component of the ENSO teleconnection dominates during a particular event. Figure 9 suggests that EP events (e, f) have a larger influence on the non-NAO ENSO signal over the North Atlantic sector than CP events (a, b). This is consistent with extreme El Niños having non-NAO teleconnections, as these events mainly consist of very strong EP-El Niños. However, this explanation is not completely satisfactory because EP-El Niño teleconnection is also found to have an NAO-related component (Fig. 9g).

If considering the composites in terms of El Niño minus La Niña (as in Sects. 3.1, 3.2), CP-ENSO (Fig. 9c, d) has a much stronger relationship to the NAO than EP-ENSO (Fig. 9g, h) (see also Calvo et al. 2017; Feng et al. 2017; Graf and Zanchettin 2012; Ren et al. 2019) because EP-La Niña teleconnection has the same sign as for EP-El Niño, as already described (thus panel c minus d is stronger than panel g minus h). Although not all the patterns in Fig. 9 are statistically significant, the EP-La Niña result in panel h could explain why full ENSO composites or linear regressions lack a clear NAO signal as these events together actually reduce the NAO anomaly in these types of analyses.

4 Summary and discussion

In a recent study, Mezzina et al. (2020) questioned whether ENSO has a connection to the NAO as is commonly reported (El Niño associated with negative NAO, La Niña associated with positive NAO). Their main argument relies on apparent differences between the upper-level atmospheric fields associated with ENSO and those associated with the NAO. If confirmed, the study could have ramifications on not only our fundamental understanding of ENSO teleconnections, but also in applied areas such as model evaluation and climate prediction.

Our study examines the above claim further. We do this by identifying ENSO signals in atmospheric data that have been first decomposed into components which are orthogonal and parallel to the NAO. This formal decomposition allows us to unambiguously identify non-NAO and NAO portions of the ENSO teleconnection. The composite results (El Niño minus La Niña) show that the well-known wave-train in the North Pacific resides in the non-NAO part of the teleconnection (bottom row of Fig. 2). Importantly, analysis of the NAO-related data shows statistically significant signals in JFM (bottom row of Fig. 3). Additional statistical tests using bootstrapping (Figs. 4, 10) confirm the widely reported relationship between ENSO and the NAO at the 95% confidence level. The main conclusion is that both the non-NAO and NAO variabilities are embedded in the canonical ENSO teleconnection patterns at upper atmospheric levels (Fig. 10 and Sect. 3.1).

A possible objection to the methodology used here (García-Serrano 2022, personal communication) is that the NAO index (PC 1 of SLP over a North Atlantic sector) intrinsically includes a statistical co-variability with Niño3.4 time series, and hence shared dipolar teleconnection structure, but that of which Mezzina et al. (2020) argues has no other NAO properties. Therefore, the current study may not resolve the debate fully. However, in attempting to understand the NAO, its dynamics and teleconnection effects, one must first define the NAO in terms of its spatial structure (meridional dipole) and associated variability (principal component or index). One cannot get away with such procedures when doing statistical analyses of noisy climate data. Mezzina et al. (2020) had to use the same NAO definition to put forward their arguments by comparing between upper atmospheric level teleconnections due to NAO (PC1) and Niño3.4 while the two indices co-vary and have signals of each other mixed in. Thus, a key to moving forward on this debate could be agreeing on what definition of the NAO is appropriate for the question at hand.

Circulation anomalies in Nov–Dec that lead the NAO-related ENSO teleconnection in JFM resemble the

Scandinavian pattern with a strong anticyclonic centre over the Ural (bottom row in Fig. 5). The associated meridional heat flux v*T* is mostly in phase spatially with and hence enhances the climatological pattern over the North Pacific, Arctic and Barents Sea (Fig. 6d). These characteristics have also been reported by a number of studies investigating atmospheric precursors or drivers (sea ice, Eurasian snow cover, North Atlantic SST) of the NAO, Arctic Oscillation, and polar vortex variability (e.g., Garfinkel et al. 2010; Jiménez-Esteve and Domeisen 2018; Kuroda and Kodera 1999; Takaya and Nakamura 2008; García-Serrano et al. 2015; Gastineau et al. 2017; Siew et al. 2020). These related atmospheric properties provide support for the stratospheric pathway by which ENSO influences the NAO.

The existence of the non-NAO and NAO-related ENSO teleconnections likely contributes to non-linearities being detected by many studies. The clearest demonstration comes from extreme El Niño events, whose teleconnection (Sect. 3.3) is found to be essentially a non-NAO phenomenon with a contemporaneous interaction with the stratosphere in JFM. Other than the role of extreme El Niño events (possibly involving also the tropical Atlantic, seeToniazzo and Scaife 2006; Hardiman et al. 2019), it is not completely clear from analyses we have performed which other factors determine whether the non-NAO or NAO variability is active during a typical ENSO event (Sect. 3.3). Previous studies have suggested that ENSO SST types, atmospheric and oceanic states over the Indian and tropical Atlantic oceans, and the stratospheric polar vortex could modulate the ENSO teleconnections generated over the North Atlantic. Climate change and multidecadal climate variation can also modulate the strength of the ENSO-NAO relationship (e.g., Fereday et al. 2020; Ivasic et al. 2021; López-Parages et al. 2014; López-Parages and Rodríguez-Fonseca 2012). Viewed in the context of our results, these factors could be further investigated in terms of how they modulate the ENSO teleconnection to the North Atlantic, and thus when it manifests as an NAO-related or non-NAO signal. Improved understanding of the modulating factors could contribute to better dynamical understanding of Euro-Atlantic variability, more targeted metrics for climate model evaluation, and improved accuracy of seasonal predictions. Our study demonstrates the benefits of separating the atmospheric variability into the non-NAO and NAO components in the research of ENSO teleconnection.

Appendix

See Figs. 10, 11, 12 and 13.
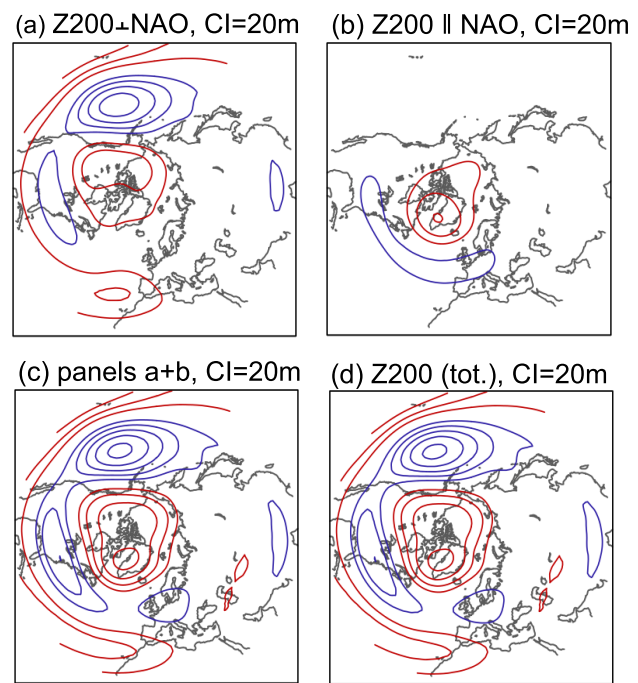
Fig. 10 **a** JFM Z200 composite for ENSO using data with variability orthogonal to NAO (left), and **b** parallel to NAO. Extreme El Ninos are excluded. These are exactly the same as Figs. 2f and 3f except CI = 20 m. **c** Sum of panels (**a**, **b**). **d** Same as panels **a**, **b** except for the original (i.e., unfiltered) data. Blue (red) contour lines indicate negative (positive) anomalies
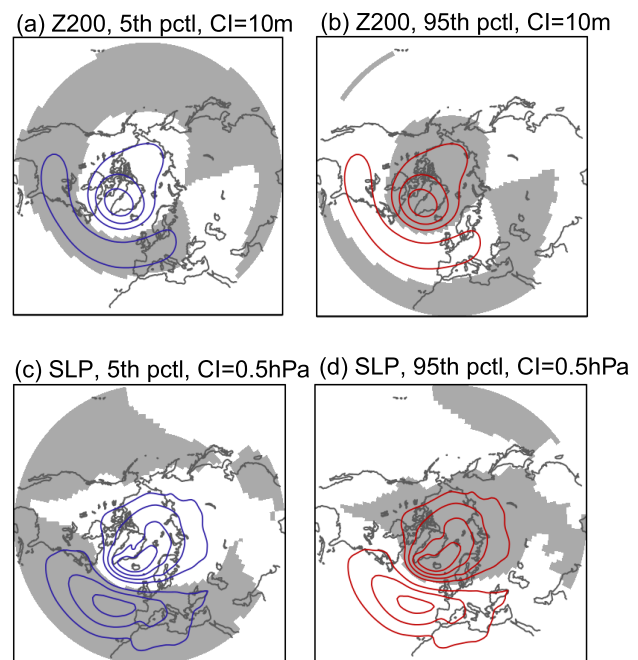

Fig. 11 Shown in contour lines are the grid-point 5th and 95th percentile values in the 2000 bootstrap composites for JFM. Each bootstrap composite is the average Z200 (or SLP) from randomly selected 23 years minus the same from randomly selected 33 years in 1870–2014. The variability parallel to NAO are analysed here. Blue (red) contour lines indicate negative (positive) anomalies. The grey shading indicates where the observed ENSO composite (Fig. 3e, f) is less (greater) than the 5th (95th) percentile. Original data: NOAA-CIRES Twentieth Century Reanalysis (V2c)

Fig. 12 Atmospheric fields composites in ND for extreme El Niños events (1878, 1889, 1973, 1983, 1998) in JFM, i.e. composites are leading El Niños. Left: total ND variability, middle: ND variability orthogonal to NAO in JFM, right: ND variability parallel to NAO in JFM. Blue (red) contour lines indicate negative (positive) anomalies. The grey shading indicates statistical significance level at 5%. Original data: NOAA-CIRES Twentieth Century Reanalysis (V2c)
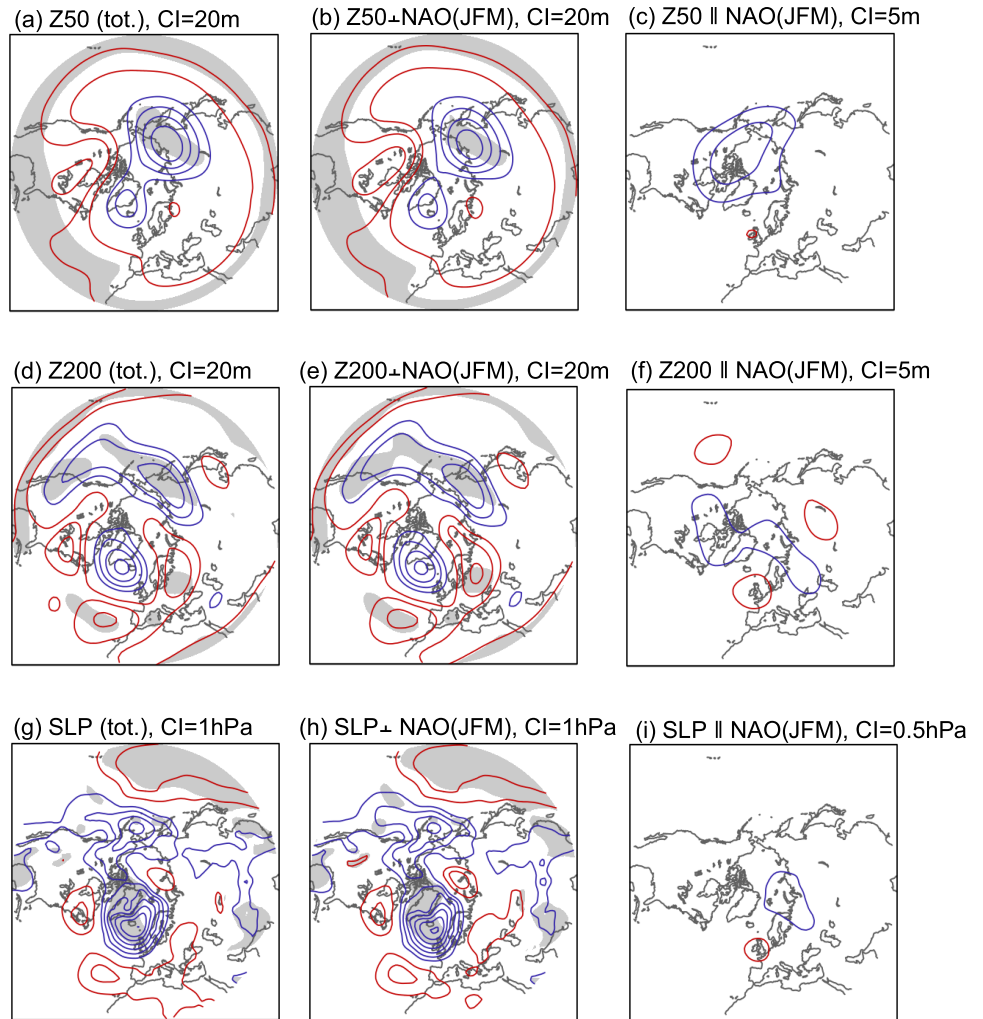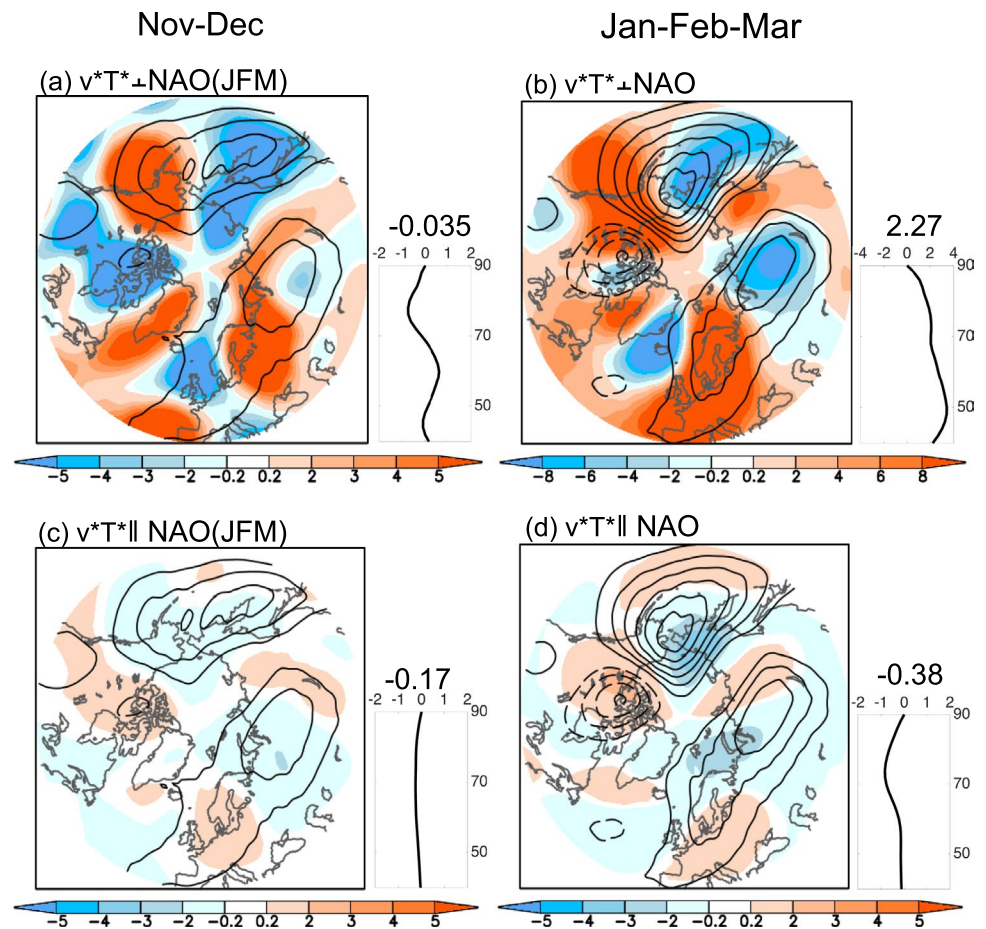
Supplementary Information The online version contains supplementary material available at https://doi.org/10.1007/s00382-023-06697-8.

Data availability Scripts and data that can be used for replicating the reported analyses and figures are archived at https://doi.org/10.5281/zenodo.6415163. NOAA-CIRES Twentieth Century Reanalysis (V2c) data are available at https://www.psl.noaa.gov/data/gridded/data. 20thC_ReanV2c.html and the HadISST1.1 data at https://www.metoffice.gov.uk/hadobs/hadisst/.

Declarations

Conflict of interest The authors have no competing interests to declare.

References

Abid MA, Kucharski F, Molteni F, Kang IS, Tompkins AM, Almazroui M (2021) Separating the Indian and Pacific Ocean impacts on the Euro-Atlantic response to ENSO and its transition from

early to late winter. J Clim 34:1531–1548. https://doi.org/10.1175/JCLI-D-20-0075.1

Ashok K, Behera SK, Rao SA, Weng H, Yamagata T (2007) El Niño Modoki and its possible teleconnection. J Geophys Res (Oceans) 112:C11007. https://doi.org/10.1029/2006JC003798

Ayarzagüena B, Ineson S, Dunstone N, Baldwin MP, Scaife AA (2018) Intraseasonal effects of El Niño-Southern Oscillation on North Atlantic climate. J Clim 31:8861–8873. https://doi.org/10.1175/JCLI-D-18-0097.1

Barnston AG, Livezey RE (1987) Classification, seasonality and persistence of low-frequency atmospheric circulation patterns. Mon Weather Rev 115:1083–1126. https://doi.org/10.1175/1520-0493(1987)115%3c1083:CSAPOL%3e2.0.CO;2

Bayr T, Domeisen DIV, Wengel C (2019) The effect of the equatorial Pacific cold SST bias on simulated teleconnections to the North Pacific and California. Clim Dyn 53:3771–3789. https://doi.org/10.1007/s00382-019-04746-9

Bell CJ, Gray LJ, Charlton-Perez AJ, Joshi MM, Scaife AA (2009) Stratospheric communication of El Niño teleconnections to European winter. J Clim 22:4083–4096. https://doi.org/10.1175/2009JCLI2717.1

Brönnimann S, Xoplaki E, Casty C, Pauling A, Luterbacher J (2007) ENSO influence on Europe during the last centuries. Clim Dyn 28:181–197. https://doi.org/10.1007/s00382-006-0175-z

Bueh C, Nakamura H (2007) Scandinavian pattern and its climatic impact. Q J R Meteorol Soc 133:2117–2131. https://doi.org/10.1002/qj.173

Butler AH, Polvani LM, Deser C (2014) Separating the stratospheric and tropospheric pathways of El Niño-Southern Oscillation teleconnections. Environ Res Lett 9:024014. https://doi.org/10.1088/1748-9326/9/2/024014

Cagnazzo C, Manzini E (2009) Impact of the stratosphere on the winter tropospheric teleconnections between ENSO and the North Atlantic and European Region. J Clim 22:1223–1238. https://doi.org/10.1175/2008JCLI2549.1

Calvo N, Iza M, Hurwitz MM, Manzini E, Peña-Ortiz C, Butler AH, Cagnazzo C, Ineson S, Garfinkel C (2017) Northern hemisphere stratospheric pathway of different El Niño flavors in CMIP5 models. J Clim. https://doi.org/10.1175/JCLI-D-16-0132.1

Casselman JW, Jiménez-Esteve B, Domeisen DIV (2022) Modulation of the El Niño teleconnection to the North Atlantic by the tropical North Atlantic during boreal spring. Weather Clim Dyn 3:1077–1096. https://doi.org/10.5194/wcd-3-1077-2022

Compo GP et al (2011) The Twentieth Century Reanalysis project. Q J R Meteorol Soc 137(1):28. https://doi.org/10.1002/qj.776

Deser C, Simpson IR, McKinnon KA, Phillips AS (2017) The Northern Hemisphere extra-tropical atmospheric circulation response to ENSO: How well do we know it and how do we evaluate models accordingly? J Clim 30:5059–5082. https://doi.org/10.1175/JCLI-D-16-0844.1

Domeisen DIV, Garfinkel CI, Butler AH (2019) The teleconnection of El Niño-Southern Oscillation to the stratosphere. Rev Geophys 57:5–47. https://doi.org/10.1029/2018RG000596

Feng J, Chen W, Li Y (2017) Asymmetry of the winter extra-tropical teleconnections in the Northern Hemisphere associated with two types of ESNO. Clim Dyn 48:2135–2151. https://doi.org/10.1007/s00382-016-3196-2

Fereday DR, Chadwick R, Knight JR, Scaife AA (2020) Tropical rainfall linked to stronger ENSO-NAO teleconnection in CMIP5 models. Geophys Res Lett 47:e2020GL088664. https://doi.org/10.1029/2020GL088664

Garcia-Herrera R, Calvo N, Garcia RR, Giorgetta MA (2006) Propagation of ENSO temperature signals into the middle atmosphere: a comparison of two general circulation models and ERA-40 reanalysis data. J Geophys Res (Atmos) 111:D06101. https://doi.org/10.1029/2005JD006061

García-Serrano J, Frankignoul C, Gastineau G, de la Camara A (2015) On the predictability of the winter Euro-Atlantic climate: lagged influence of autumn Arctic sea ice. J Clim 28:5195–5216. https://doi.org/10.1175/JCLI-D-14-00472.1

Garfinkel CI, Hartmann HL (2008) Different ENSO teleconnections and their effects on the stratospheric polar vortex. J Geophys Res 113:D18114. https://doi.org/10.1029/2008JD009920

Garfinkel CI, Hartmann DL, Sassi F (2010) Tropospheric precursors of anomalous Northern Hemisphere stratospheric polar vortex. J Clim 23:3282–3299. https://doi.org/10.1175/2010JCLI3010.1

Gastineau G, García-Serrano J, Frankignoul C (2017) The influence of autumnal Eurasian snow cover on climate and its link with Arctic sea ice cover. J Clim 30:7599–7619. https://doi.org/10.1175/JCLI-D-16-0623.1

Gill AE (1980) Some simple solutions for heat-induced tropical circulations. Q J R Meteorol Soc 106:447–462. https://doi.org/10.1002/qj.49710644905

Graf H-F, Zanchettin D (2012) Central Pacific El Niño, the "subtropical bridge", and Eurasian climate. J Geophys Res (Atmos) 117:D01102. https://doi.org/10.1029/2011JD016493

Hardiman SC, Dunstone NJ, Scaife AA, Smith DM, Ineson S, Lim J, Fereday D (2019) The impact of strong El Niño and La Niña events on the North Atlantic. Geophys Res Lett 46:2874–2883. https://doi.org/10.1029/2018GL081776

Hoskins BJ, Ambrizzi T (1993) Rossby wave propagation on a realistic longitudinally varying flow. J Atmos Sci 50:1661–1671. https://doi.org/10.1175/1520-0469(1993)050%3c1661:RWPOAR%3e2.0.CO;2

Hoskins BJ, Karoly D (1981) The steady linear response of a spherical atmosphere to thermal and orographic forcing. J Atmos Sci 38:1179–1196. https://doi.org/10.1175/1520-0469(1981)038%3c1179:TSLROA%3e2.0.CO;2

Ineson S, Scaife AA (2009) The role of stratosphere in the European climate response to El Niño. Nat Geosci 2:32–36. https://doi.org/10.1038/ngeo381

Ivasić S, Herceg-Bulić I, King MP (2021) Recent weakening in the winter ENSO teleconnection over the North Atlantic-European region. Clim Dyn 57:1953–1972. https://doi.org/10.1007/s00382-021-05783-z

Iza M, Calvo N, Manzini E (2016) The stratospheric pathway of La Nina. J Clim 29:8899–8914. https://doi.org/10.1175/JCLI-D-16-0230.1

Jiménez-Esteve B, Domeisen DIV (2018) The tropospheric pathway of the ENSO-North Atlantic teleconnection. J Clim 31:4563–4584. https://doi.org/10.1175/JCLI-D-17-0716.1

Jiménez-Esteve B, Domeisen DIV (2020) Nonlinearity in the tropospheric pathway of ENSO to the North Atlantic. Weather Clim Dyn 1:225–245. https://doi.org/10.5194/wcd-1-225-2020

Jin F, Hoskins BJ (1995) The direct response to tropical heating in a baroclinic atmosphere. J Atmos Sci 52(3):307–319. https://doi.org/10.1175/1520-0469(1995)052%3c0307:TDRTTH%3e2.0.CO;2

King MP, Herceg-Bulic I, Bladé I, García-Serrano J, Keenlyside N, Kucharski F, Li C, Sobolowski S (2018a) Importance of late fall ENSO teleconnection in the Euro-Atlantic sector. Bull Am Meteorol Soc 99:1337–1343. https://doi.org/10.1175/BAMS-D-17-0020.1

King MP, Herceg-Bulic I, Kucharski F, Keenlyside N (2018b) Interannual tropical Pacific sea surface temperature anomalies teleconnection to Northern Hemisphere atmosphere in November. Clim Dyn 50:1881–1899. https://doi.org/10.1007/s00382-017-3727-5

King MP, Yu E, Sillmann J (2020) Impact of strong and extreme El Niños on European hydroclimate. Tellus A 72:1–10. https://doi.org/10.1080/16000870.2019.1704342

King MP, Li C, Sobolowski S (2021) Resampling of ENSO teleconnections: accounting for cold-season evolution reduces uncertainty in the North Atlantic. Weather Clim Dyn 2:759–776. https://doi.org/10.5194/wcd-2-759-2021

Kuroda Y, Kodera K (1999) Role of planetary waves in the stratosphere-troposphere coupled variability in the Northern Hemisphere. Geophys Res Lett 26:2375–2378. https://doi.org/10.1029/1999GL900507

López-Parages J, Rodríguez-Fonseca B (2012) Multidecadal modulation of El Niño influence on the Euro-Mediterranean rainfall. Geophys Res Lett 39(2):1–7. https://doi.org/10.1029/2011GL050049

López-Parages J, Rodríguez-Fonseca B, Terray L (2014) A mechanism for the multidecadal modulation of ENSO teleconnection with Europe. Clim Dyn 45:867–880. https://doi.org/10.1007/s00382-014-2319-x

Manzini E, Giorgetta MA, Esch M, Kornblueh L, Roeckner E (2006) The influence of sea surface temperatures on the northern winter stratosphere: ensemble simulations with the MAECHAM5 model. J Clim 19:3863–3881. https://doi.org/10.1175/JCLI3826.1

Mezzina B, García-Serrano J, Bladé I, Kucharski F (2020) Dynamics of the ENSO teleconnection and NAO variability in the North-Atlantic-European late winter. J Clim 33:907–923. https://doi.org/10.1175/JCLI-D-19-0192.1

Michel C, Li C, Simpson IR, Bethke R, King MP, Sobolowski S (2020) The change in the ENSO teleconnection under a low global warming scenario and the uncertainty due to internal variability. J Clim 33:4871–4889. https://doi.org/10.1175/JCLI-D-19-0730.1

Molteni F, Roberts CD, Senan R, Keeley SPE, Bellucci A, Corti S, Franco RF, Haarsma R, Levine X, Putrasahan D, Robers MJ, Terray L (2020) Boreal-winter teleconnections with tropical Indo-Pacific rainfall in HighResMIP historical simulations from the PRIMAVERA project. Clim Dyn 55:1843–1873. https://doi.org/10.1007/s00382-020-05358-4

Moron V, Gouirand I (2003) Seasonal modulation of the El Niño-Southern Oscillation relationship with sea level pressure anomalies over the North Atlantic in October–March 1873–1996. Int J Climatol 23:143–155. https://doi.org/10.1002/joc.868

Peings Y (2019) Ural blocking as a driver of early-winter stratospheric warmings. Geophys Res Lett 46:5460–5468. https://doi.org/10.1029/2019GL082097

Rayner NA, Parker DE, Horton EB, Folland CK, Alexander LV, Rowell DP, Kent EC, Kaplan A (2003) Global analyses of sea surface temperature, sea ice, and night marine air temperature since the late nineteenth century. J Geophys Res (Atmos) 108:4407. https://doi.org/10.1029/2002JD002670

Ren H-L, Scaife AA, Dunstone N, Tian B, Liu Y, Ineson S, Lee J-Y, Smith D, Liu C, Thompson V, Vellinga M, MacLachlan C (2019) Seasonal predictability of winter ENSO types in operational dynamical model predictions. Clim Dyn 52:3869–3890. https://doi.org/10.1007/s00382-018-4366-1

Sardeshmukh PD, Hoskins BJ (1988) The generation of global rotational flow by steady idealized tropical divergence. J Atmos Sci 45:1228–1251. https://doi.org/10.1175/1520-0469(1988)045%3c1228:TGOGRF%3e2.0.CO;2

Scaife AA, Arribas A, Blockley E, Brookshaw A, Clark RT, Dunstone N, Eade R, Fereday D, Folland CK, Gordon M, Hermanson L, Knight JR, Lea DJ, MacLachlan MA, Martin M, Peterson AK, Smith D, Vellinga M, Wallace E, Waters J, Williams A (2014) Skillful long-range prediction of European and North American winters. Geophys Res Lett 41:2514–2519. https://doi.org/10.1002/2014GL059637

Scaife AA, Comer R, Dunstone N, Fereday D, Folland C, Good E, Gordon M, Hermanson L, Ineson S, Karpechko A, Knight J, MacLachlan C, Maidens A, Peterson KA, Smith D, Slingo J, Walker B (2017) Predictability of European winter 2015/16. Atmos Sci Lett 18:38–44. https://doi.org/10.1002/asl.721

Siew PYS, Li C, Sobolowski SP, King MP (2020) Intermittency of Arctic-mid-latitude teleconnections: stratospheric pathway between autumn sea ice and the winter North Atlantic Oscillation. Weather Clim Dyn 1:261–275. https://doi.org/10.5194/wcd-1-261-2020

Taguchi M, Hartmann DL (2006) Increased occurrence of stratospheric sudden warmings during El Niño as simulated by WACCM. J Clim 19:324–332. https://doi.org/10.1175/JCLI3655.1

Takaya K, Nakamura H (2008) Precursory changes in planetary wave activity for midwinter surface pressure anomalies over the Arctic. J Meteorol Soc Jpn 86:415–427. https://doi.org/10.2151/jmsj.86.415

Toniazzo T, Scaife AA (2006) The influence of ENSO on winter North Atlantic climate. Geophys Res Lett 33:1–5. https://doi.org/10.1029/2006GL027881

Trenberth KE, Branstator GW, Karoly D, Kumar A, Lau NC, Ropelewski C (1998) Progress during TOGA in understanding and modeling global teleconnections associated with tropical sea surface temperatures. J Geophys Res 103:14291–14324. https://doi.org/10.1029/97JC01444

White I, Garfinkel CI, Gerber EP, Jucker M, Aquila V, Oman LD (2019) The downward influence of sudden stratospheric warmings: association with the tropospheric precursors. J Clim 32:85–108. https://doi.org/10.1175/JCLI-D-18-0053.1

Weinberger I, Garfinkel CI, White IP, Oman LD (2019) The salience of nonlinearities in the boreal winter response to ENSO. Clim Dyn 53:4591–4610. https://doi.org/10.1007/s00382-019-04805-1

Zhang W, Wang Z, Stuecker M, Turner AG, Jin FF, Geng X (2018) Impact of ENSO longitudinal position on teleconnection to NAO. Clim Dyn 52:257–274. https://doi.org/10.1007/s00382-018-4135-1